ARTICLE

Bioassembled Layered Silicate-Metal Nanoparticle Hybrids

Lawrence F. Drummy,[†] Sharon E. Jones,[†] Ras B. Pandey,[‡] B. L. Farmer,[†] Richard A. Vaia,[†] and Rajesh R. Naik*,[†]

Materials and Manufacturing Directorate, Air Force Research Laboratory, Wright-Patterson AFB, Ohio 45433, and Department of Physics and Astronomy, University of Southern Mississippi, Hattiesburg, Mississippi 39406

ABSTRACT Here we report on the bioenabled assembly of layered nanohybrids using peptides identified with regard to their affinity to the nanoparticle surface. A dodecamer peptide termed M1, determined from a phage peptide display library, was found to bind to the surface of a layered aluminosilicate (montmorillonite, MMT). Fusion of a metal binding domain to the M1 peptide or the M1 peptide by itself was able to direct the growth of metal nanoparticles, such as gold and cobalt−platinum, respectively, on the MMT. This method of producing hybrid nanoclay materials will have utility in catalytic, optical, biomedical, and composite materials applications.

KEYWORDS: phage display • peptide • montmorillonite • nanoclay • CoPt • bionanotechnology

There is growing interest in assembling disparate materials in order to obtain synergistic properties or impart additional functionality. Several examples have demonstrated the usefulness of using molecular building blocks such as proteins (1), peptides (2) and nucleic acids (3, 4) for designed organization of hybrid nanostructures. These hybrid structures have been shown to have interesting catalytic, sensing, and optical properties. For example, peptides identified from combinatorial libraries have been shown to strongly bind to nanomaterials, specifically interacting with certain crystallographic surfaces (5), and they can be used as biolinkers or molecular erectors to direct the assembly of disparate materials into predefined architectures (6). Bifunctional peptides have been used to assemble bimetallic catalytic nanostructures (2) as well as to spatially control the deposition of nanoparticles onto substrates (6).

In this study, we demonstrate a method to functionalize the surface of layered aluminosilicate nanoparticles with metal nanoparticles using peptides identified from a peptide library. Layered aluminosilicate materials, such as montmorillonite (MMT), have been investigated for applications as diverse as polymer nanocomposites (7), drug delivery (8), sorption (9), filtration (10), protein fractionation (11), sensing (12), hemostatic agents (13) and enzyme immobilization (14). Several of these application areas would benefit from a biological "handle" to increase the functionality of the layered silicate, and peptides are an ideal candidate for providing this handle because of their wide array of chemical functionalities. The interactions between layered silicates and amino acids (15, 16), proteins (17), and enzymes (18) have been extensively examined in the context of prebiotic peptide synthesis, soil chemistry, and environmental pollution, but only recently with regard to creating functional materials (19, 20). The specific binding affinity provided by the phage indentified peptide sequence enables precise, single-pot assembly of hybrid layered nanostructures, such as Au or superparamagnetic CoPt nanoparticle decorated aluminosilicate layers. Relative to MMT, the functionality of these hybrid nanoparticles are substantially increased, for example, being responsive to a weak external magnetic field that enables novel magneto-optical fluids, as well as noncontact control of nanolayer morphology during processing or heating during exposure to RF radiation.

RESULTS AND DISCUSSION

Montmorillonite (MMT)-binding peptides were identified from a dodecamer M13 phage peptide library using standard biopanning methods (50 mM Tris-HCl pH 7.5, 150 mM NaCl, with a maximum stringency of 0.6% Tween). Specifically, the M13 library was tested for binding against three purified, homoionic montmorillonites derived from the same source mineral (Southern Clay Products, 92 meq/100 g, $Na_{0.66}[Si_{7.8}Al_{0.2}O_{16}][Al_{2.96}Fe_{0.45}Mg_{0.44}Ca_{0.02}\square_{0.13}O_4(OH)_4]$) (21): a hydrophilic sodium MMT (NaMMT, $d_{001} = 1.13$ nm), and two organophillic montmorillonites differing only in the structure of the cation (octyldecyl primary ammonium MMT (pC18MMT, $d_{001} = 1.75$ nm) and octyldecyl trimethyl quaternary ammonium MMT (qC18MMT, $d_{001} = 1.80$ nm)). In addition to the oxygen-rich lamella surface, montmorillonite has two types of charges: (1) layer charge that originates from isomorphic substitutions within the aluminosilicate lattice and (2) pH-dependent charges on the lamellae edges that originate from aluminum and silicon hydroxide associated with the incompletely condensed terminal silicon- and oxygen-containing tetrahedra and aluminum- and oxygen-containing octahedra (22). These layer charges are neutralized by cations (23, 24). Note that because phage binding is

* Corresponding author. E-mail: rajesh.naik@wpafb.af.mil.
Received for review February 8, 2010 and accepted March 31, 2010
[†] Air Force Research Laboratory.
[‡] University of Southern Mississippi.
DOI: 10.1021/am1001184

Published on Web 04/20/2010

Table 1. Phage Display Sequence Results for Na^+ MMT, Primary Ammonium C18 Modified MMT, and Quaternary Ammonium C18 Modified MMT. Legend: Red, Positively Charged; Gray, Negatively Charged; Blue, Hydroxyl; Gold, Hydrophobic

Na^+ MMT binding peptide	Sequence	pI
M1	HGINTTKPFKSV	10.5
M2	WPSSYLSPIPYS	6.0
M3	AVTTLTLVPAGT	6.0
M4	ALTGSTKSAFGG	10.1

Prim. Amm. MMT bind. pep.	Sequence	pI
M1	HGINTTKPFKSV	10.5
PM1	TSVRTHFPLYPV	9.8
PM2	GFEHKDQRFTRE	7.8

Quat. Amm. MMT bind. pep.	Sequence	pI
M1	HGINTTKPFKSV	10.5
QM1	GTFPLAIKARDP	10.1
QM2	LHLPSDRLRLWG	10.9
QM3	MHRSDLMSAAVR	10.9

a surface event, the standard biopanning method provides selectivity toward the external surface of the crystallite in contact with the aqueous media, whether that surface is hydrophilic or hydrophobic. For the MMTs examined, the available surface area per mass for phage binding to the organophillic pC18MMT and q2C18MMT will be substantially less than for the highly water swellable NaMMT. Nevertheless, the size of the secondary particles, whether encompassing hundreds of aluminosilicate layers for pC18MMT and q2C18MMT or two to three layers for NaMMT, will not substantially impact the surface energy and molecular-level processes at the external water−MMT interface.

Table 1 summarizes the peptides identified after six competitive cycles, using the single-letter amino acid notation, color-coded for the functional nature of the R-group. A unique phage clone with the displayed peptide sequence His-Gly-Ile-Asn-Thr-Thr-Lys-Pro-Phe-Lys-Ser-Val (termed M1) was identified for all three MMT targets. When a negatively charged residue is found, it is adjacent to a cationic or hydroxyl-containing residual, effectively shielding its long-range electrostatic character. Also, the isoelectric pH, (pI) (25), for each peptide is above 7, with the exception of two MMT sequences (M2 and M3) that are devoid of cationic residues and dominated by hydroxyl pendants. The high pIs indicate a net cationic character at neutral pH, and where the biopanning was conducted. Overall, these sequences are consistent with selection based on a displacement exchange with the initial cations on the MMT surface. The commonality of the M1 for all three Mts, implies that its affinity is greater than an alkali metal ion, primary ammonium or quaternary ammonium cation. For displacement and competitive exchange on MMT (26), monovalent organic cations compete with inorganic cations for adsorption and are usually more tightly held, apparently because of the supplemental effect of van der Waals forces between the absorbed organic groups (27). The additional entropic factors and constraint to dynamic motion arising from covalent coupling of multiple cationic groups further favors polycationic absorption. Streric hindrance between very large cations however, is known to limit complete exchange (23, 28). Finally,

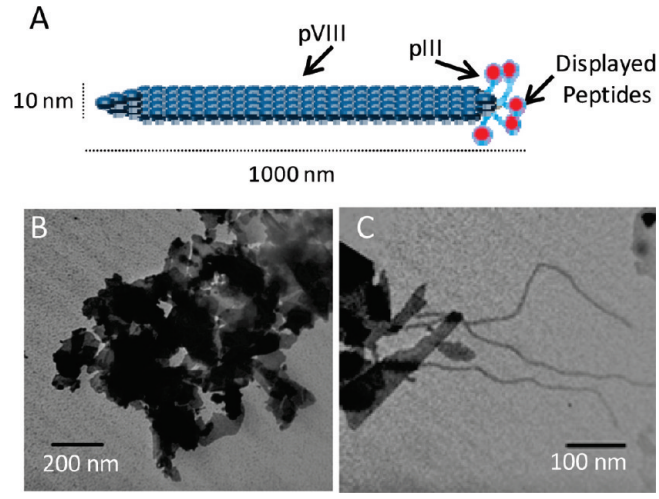

FIGURE 1. (A) Schematic illustration of the M13 bacteriophage showing the displayed peptides on the pIII coat protein. Low-voltage transmission electron microscope (LVTEM, 5 kV) micrograph of MMT sheets incubated with (B) phage displaying a non-specific peptide or (C) phage displaying the M1 peptide. Note the phages displaying the M1 peptide attach to the MMT sheets. The phages are unstained.

the unique hydroxyl dominated motifs observed for NaMMT and not for pC18MMT and qC18MMT likely reflects the additional absorptive processes possible for alkali metal MMTs: cation chelation (27). The differences between all these sequences are currently under investigation; for the present study, the M1 peptide will be the focus.

Low-voltage transmission electron microscopy (LVTEM) of NaMMT particles with the biopanned phage clones qualitatively showed selective binding to the aluminosilicate layers (Figure 1). For example, the phage clone expressing M1 exhibited binding to the MMT sheets (Figure 1C), whereas the M13 phage displaying a non-specific peptide showed little or no binding to the MMT (Figure 1B). We noted in several of the TEM images that the ends of the phages attached to the MMT sheets because of the peptide being expressed on the pIII coat protein at the terminus of the M13. In a few regions, we did observe the MMT sheet interacting with the M13 phage along its long axis, possibly via the pVIII coat. The external surface of the pVIII coat protein contains 11% Lys residues (29), which are likely to interact favorably with the NaMMT. However, as implied by the convergence of peptide sequences during the biopanning and the control M13 behavior, the stringent washing conditions applied after initial binding negates the weaker non-specific pVIII-MMT interactions in favor of the strong pIII protein interactions via the displayed peptide. Therefore, the small number of axial M13−MMT interactions is likely the result of phage lying down on top of the MMT during sample preparation.

The dodecamer M1 peptide (MW 1328 g/mol) with N and C termini was synthesized via standard solid-state methods based on the DNA sequence of the pIII gene of the M1 phage clone, and several peptide binding assays were carried out. X-ray diffraction of the resulting intercalation compound between the M1 peptide and NaMMT revealed the interlayer spacing and aspects of peptide confirmation on the alumi-

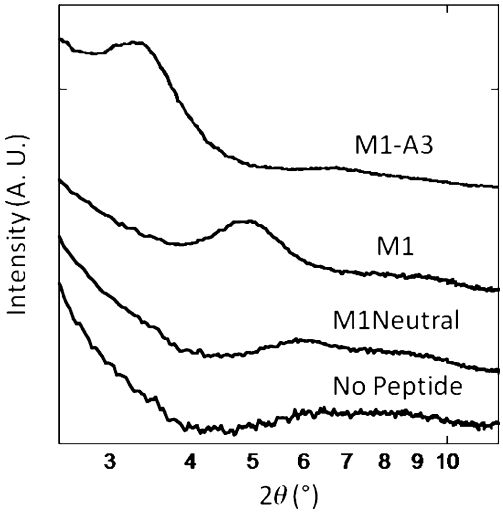

FIGURE 2. Powder X-ray diffraction patterns of the MMT bound with peptides in solution and then dried into a powder. The curve with a peak near 7° corresponds to the control MMT with no peptide, which underwent the same washes as the samples with peptide, in order to remove nonspecific binders.

nosilicate surface. All intercalation reactions were prepared with one peptide molecule per MMT cation exchange site (0.092 mols per 100 g of MMT), followed by washing and centrifugation to remove unbound or nonspecifically bound peptide, and subsequent drying into a powder. The polycationic nature of M1 implies the exchange reaction is conducted with a molar excess of intercalant. As demonstrated by the similar interlayer spacings for reaction with (HEPES or Tris Buffer) and without buffer, the molar excess of buffer (~50× available MMT exchange sites) does not alter the intercalate structure, nor cointercalates, from the pH 7.5 media. Additionally, the successful intercalation of M1 into NaMMT from a solution with 150× molar excess of sodium cations further confirms M1's relatively strong interaction. Figure 2 compares the basal reflections of the intercalation product of the M1 peptide to that of other select peptides. The M1−NaMMT complex exhibited an interlayer spacing of 1.8 nm, compared a broad bimodal (1.3 and 1.0 nm) peak for the control, which underwent the same dispersion and water washes but in the absence of M1 peptide. The 1.3 nm spacing in the control is consistent with a monolayer of water between the MMT layers hydrating the interlayer sodium (30), and the 1.0 nm spacing is from dry Na^+ MMT. M1Neutral was a dodecamer peptide with the same sequence as M1 except that the lysine and histidine residues were replaced with glycine. This peptide did not bind to MMT, as evidenced by the similar X-ray pattern to the control, indicating that the M1 Neutral peptide was removed during the washes. The 1.8 nm spacing, seen for M1 peptide, is consistent with other protein-MMT samples and has been attributed to a β-type molecular conformation with the biomolecules lying down flat on the MMT (001) surface (31, 32). Interestingly, this spacing is also consistent with a bilayer of alpha-ammonium alkyl chains such as seen in pC18MMT and qC18MMT (24).

To further investigate the strong binding and extended β-type conformation of M1, we applied a coarse-grained computer simulation, previously described by Pandey et al. (33) to study peptide adsorption on a hydrated montmorillonite surface (Figure 3). Details on the Monte Carlo lattice-based simulation and interaction parameters have been published (33) and are provided in the supplemental section. We find that the binding energy of Lys-7 and Lys-10 in the M1 peptide dominates the interaction with the MMT surface. The mobility profile for these residues is also lowest, confirming that the positively charged lysine residues act as the most stable anchor for M1 to MMT. In addition, the hydrogen-bonding His-1 and Asn-4 also show favorable interaction with MMT surface but with an average energy per residue 4−5 times smaller than the lysines. Overall, these simulations are consistent with the M1 experimental results, prior observations of amino-acid binding to clays (23), and pervious demonstration that the lysine resides in silk-elastin-like protein are responsible for binding to MMT surfaces (20).

Most importantly, the simulations (Figure 3) suggest that the lowest energy configuration for the M1 peptide is parallel to the MMT surface, consistent with the observed interlayer spacing. In some cases, it has been demonstrated that not only the presence of certain amino acids but their spacing and sequence is critical for strong binding, especially for crystalline atomic surfaces (34). One could argue that the emergence of M1 from the biopanning process reflects more than the presence of lysine residues; that the spacing between these residues and the overall conformation of the peptide upon interaction with the MMT platelet surface dictates its relatively strong bonding to the MMT surface. For a β conformation, the spacing between Lys-7 and Lys-10 in M1 is similar to the average spacing between charge substitution sites in the octahedral layer of the MMT used herein, 1 nm.

A combination of X-ray diffraction and TGA analysis of the washed and dried M1-MMT complex (Supporting Information) revealed the peptide content varies between 12% and 24% of the total weight, which corresponds to approximately one peptide for every 9 to 4.5 cation exchange sites on the MMT surface, respectively. The organoclays used in this study, pC18 and qC18, both have approximately the same interlayer spacing as the M1 peptide (1.8 nm), however their molecular weight is less: 270 and 318 g/mol, respectively, as compared to 1328 g/mol for M1. Because the mass of M1 is nominally 4.5 times as large as pC18 or qC18 and pC18 and qC18 both fully exchange with MMT (one molecule per cation exchange site), we expect M1 to occupy approximately 4.5 cation exchange sites on the MMT surface. TGA indicates the M1 peptide is exchanged at interlayer densities between 1× and 0.5× of the pC18/qC18 density, which is most likely due to steric effects of the larger molecule, which is commonly seen for larger organic cations such as M1 (23, 28). X-ray analysis confirmed that the interlayer spacing decreased as expected with peptide content, from 1.80 nm for a fully dense (1 M1:4.5 CEC sties) peptide bilayer to 1.48 nm for a half-density (1 M1:9 CEC sites) bilayer.

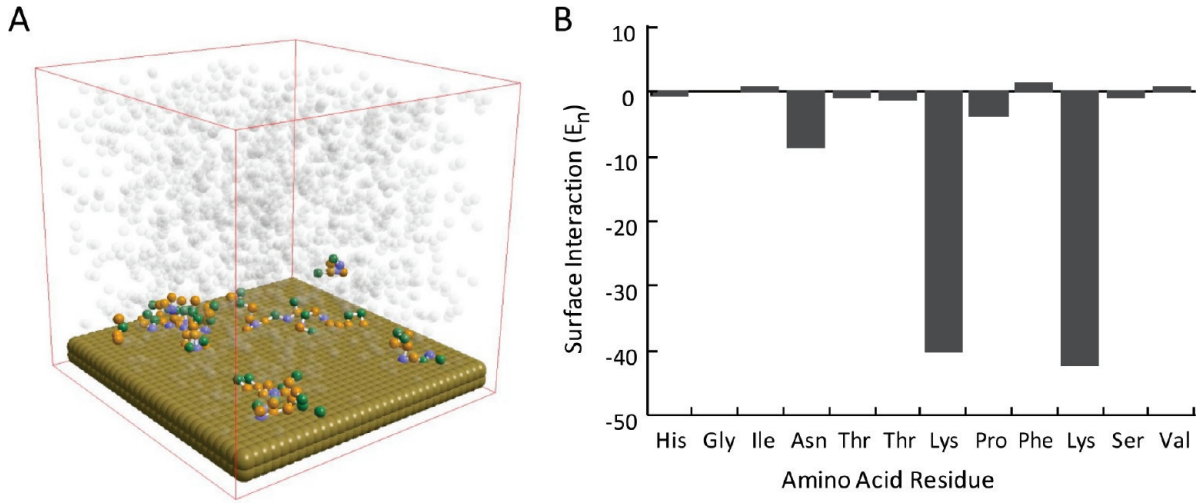

FIGURE 3. Coarse grain modeling of M1 peptide on MMT surfaces. (A) Snapshot of M1 on clay surface at the end of 1×10^5 time steps on a 64^3 cubic box. Some of the 10 chains appear fragmented because of periodic boundary conditions along the z and x directions. Solvent (water) concentration is 0.05. (dark gold, surface; green, hydrophobic; gold, polar; blue, electrostatic; gray, water). (B) Surface energy (component of E_n associated with surface interaction) of each residue in M1 peptide in arbitrary unit. Statistics: 10 peptide chains on a 64^3 lattice, each with 100 independent samples.

The binding affinity of the M1 peptide to the MMT surface was determined using fluorescence competition assays (35). Fluorescein isothiocyanate (FITC) was conjugated to the amino terminus of M1 peptide. The FITC-M1 peptide exhibited similar intercalation to NaMMT as the parent M1 by WAXS analysis. Depleted FITC-M1-MMT hybrid nanoparticles containing 1 mmol/100 g peptide were initially formed. Different concentrations of unlabeled M1 peptide were sequentially added to the depleted FITC-M1-MMT hybrids, centrifuged, and the fluorescence of the supernatant was measured to quantify the displaced amount of the FITC-M1 peptide. With different amounts of M1 added to different samples for competitive binding, and all samples starting with the same initial concentration of FITC-M1 bound to the MMT layers, varying amounts of the FITC-M1 peptide were competed off the surface of the MMT by the parent M1 peptide. The fluorescence of the supernatant increased with increasing M1 concentration according to a single site Langmuir model for which the fluorescence intensity F at a given peptide concentration P is given by (36)

$$F([P]) = \frac{F_\infty[P]}{K_d + [P]}$$

The equilibrium dissociation constant (K_d) determined from the data fit, when normalized for the initially unoccupied MMT surface area available for binding (95%), was calculated to be 35 μM for M1 peptide (see the Supporting Information, Figure S3). The interaction strength of the M1 peptide with the MMT sheet is similar to other inorganic binding peptides and materials (37, 38).

Having confirmed that the M1 peptide binds to the MMT surface, it can be used to direct nanoparticle growth, effectively decorating the surface of the aluminosilicate sheets with other inorganics. This approach has two uses: first, enabling visual confirmation of the binding sites of M1 peptide on the MMT surface, and second to serve as a method to functionalize clay nanoparticles to create hybrid nanostructures (19). Figure 4 summarizes the LVTEM images of the resulting hybrid nanostructures using the aforementioned M1-A3 fusion peptide to combine Au and MMT binding specificity. M1-A3 peptide binding to NaMMT was performed in water, the sample was washed and resuspended in 50 mM HEPES buffer pH 7.5. Gold nanoparticle synthesis was initiated by the addition of the gold salt solution (1 mM $HAuCl_4$) and incubated for 1 h at room temperature as per previous reports (39, 40). Consistent with our expectations, the gold nanoparticles were on the NaMMT surface by virtue of the gold binding A3 peptide block (Figure 4C). Figure 4C and other similar TEM images show gold binding to single MMT layers in the TEM images, not intercalated between stacked layers. Any apparent layer stacking or aggregation in the images is due to drying effects. As controls, M1 and A3 peptides by themselves were intercalated under the same reaction conditions. In both cases, no gold nanoparticles were on the MMT surface (Figure 4A,B). The M1 peptide binds to the NaMMT sheets but not to the gold nanoparticles synthesized in HEPES buffer, whereas gold nanoparticles synthesized in the absence of peptide also do not bind to the NaMMT sheet.

Note that the NaMMT sample with no peptide also showed no gold nanoparticles, confirming the critical role of the peptide to direct nanoparticle growth, and that the NaMMT surface by itself has no affinity for these gold nanoparticles. It has been demonstrated that HEPES buffer is in fact the reducing agent for $HAuCl_4$ in the $HAuCl_4$/HEPES/peptide system, and that the A3 peptide provides precise size control, binding to and stabilizing the Au^0 particles once they reach a certain size (nominally 10 nm) (40). In this case, because the A3 peptide is constrained on the MMT surface and not free in solution to bind to gold NPs, the gold mineralization process can be termed surface-directed nanoparticle growth. The gold nanoparticles are rather evenly

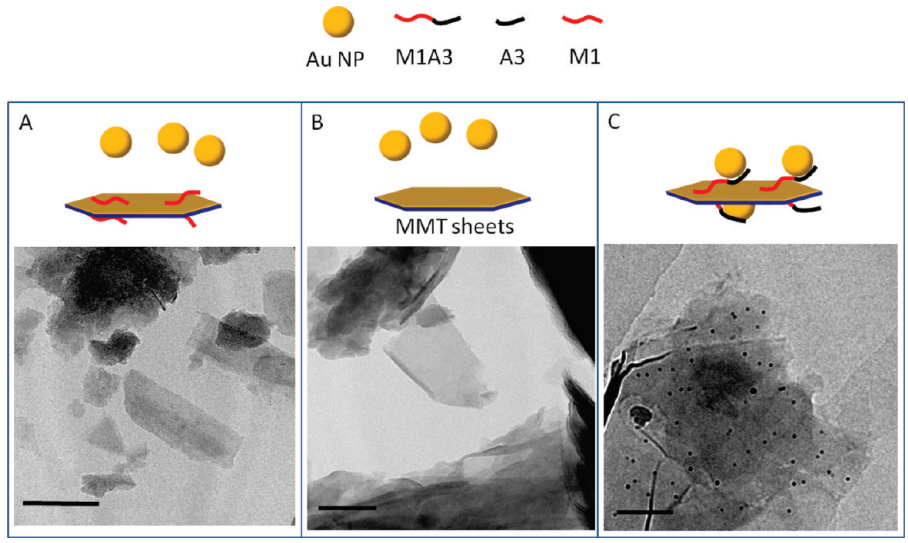

FIGURE 4. Coating MMT sheets with gold nanoparticles using the M1-A3 peptide linker. TEM micorgraphs (200 kV) image of (A) M1 peptide, (B) A3 peptide, and (C) M1-A3 peptide after gold nanoparticle synthesis in HEPES buffer. Scale bar (A, B) 500 and (C) 200 nm.

distributed across the (001) surface, with no apparent preference for binding to the NaMMT layer edges. This complements the X-ray results that indicates the M1 peptide is localized between the NaMMT layers and bound to the (001) surfaces. The preference for MMT (001) surface binding, as opposed to MMT layer edge binding, maximizes the available surface area for functionalization.

The above example of binding nanoparticles in solution to the MMT layer to create composite structures could be further exploited by room temperature synthesis of magnetic metal alloy nanoparticles using peptides. Magnetically modified MMT can be exploited in a number of ways such as in optical, structural, biochemical, wound healing or environmental applications (41, 42). Peptides have been used previously to synthesize CoPt nanoparticles (43, 44), and we constructed a fusion peptide consisting of the MMT binding M1 sequence and Co2P2, a 12 amino acid peptide previously identified to interact with CoPt nanoparticles (44). The fusion peptide M1-Co2P2 (N-His-Gly-Ile-Asn-Thr-Thr-Lys-Pro-Phe-Lys-Ser-Val-Gly-Gly-Gly-Lys-Leu-His-Ser-Ser-Pro-His-Thr-Pro-Leu-Val-Glu-OH) was able to simultaneously bind to the MMT sheets as well as CoPt.

Figure 5 shows the resulting hybrid NaMMT-CoPt nanostructures formed using the peptide linkers. The CoPt nanoparticles were synthesized using cobalt acetate and ammonium tetrachloroplatinate(II), as the precursor salts and sodium borohydride $NaBH_4$ as the reducing agent. In contrast to the M1-A3 results, both NaMMT-M1-Co2P2 peptide and NaMMT-M1 peptide complexes were capable of binding to the CoPt particles formed in solution. This is consistent with the high degree of similarity between the amino acid residues of M1 and Co2P2 peptides, relative to between M1 and A3. It is also of practical interest (ease of peptide synthesis, purity, and cost) to use the shortest peptide possible to obtain the desired result (in this case simultaneous NaMMT and CoPt binding). Interestingly, M1 peptide alone, when in the presence of Co and Pt salt precursors and an external reducing agent, does not precipitate nanoparticles at the same precursor concentration, presumably because the clay surface acts to modify the local precursor concentration, or change the local pH slightly, pushing the reaction into a different regime. NaMMT minus peptide incubated with Co and Pt salt precursors followed by reduction with sodium borohydride failed to form CoPt-MMT nanohybrids, but rather formed CoPt nanoparticles that were easily separated from the NaMMT. It is only when the solution contains the M1 peptide bound to the MMT surfaces that CoPt—MMT nanohybrids form. This result demonstrates that the biotemplate is necessary for the formation of CoPt nanoparticles on the MMT surface.

The crystal structure of CoPt nanoparticles formed with MMT-M1 is FCC, with no atomic ordering of the tetragonal L_10 phase (45) evident in X-ray or electron diffraction patterns. The morphology consists generally of 4 nm single crystalline domain nanoparticles which are often associated into 20 nm clusters (see the Supporting Information, Figure S4). Magnetic property measurements (zero-field-cooled/field-cooled experiments) on the hybrid MMT-CoPt nanostructures revealed they were superparamagnetic with a relatively high blocking temperature of ~120 K (Figure 5D), slightly higher than previously measured for CoPt/Au core/shell superparamagnetic nanoparticles (46). Superparamagnetic nanoparticles with magnetic properties similar to CoPt have been used in the so-called ferrofluids, which demonstrate unique responses to external magnetic fields, and intricate control over their alignment and aggregation state can be achieved (47). Making use of the hybrid particles response to an external field, we demonstrated a simple optical switch that exhibits magnetically controlled optical properties (Figure 6). Initially, in the presence of the magnetic field (0.2 T), nanoparticles translate toward the edges of the capillary and out of the field of view of the optical detector, and concurrently the transmitted light intensity increases. When the field is removed, the nanoparticles that have been pulled out of the light path move back into the field of view, subsequently blocking the light path, and the

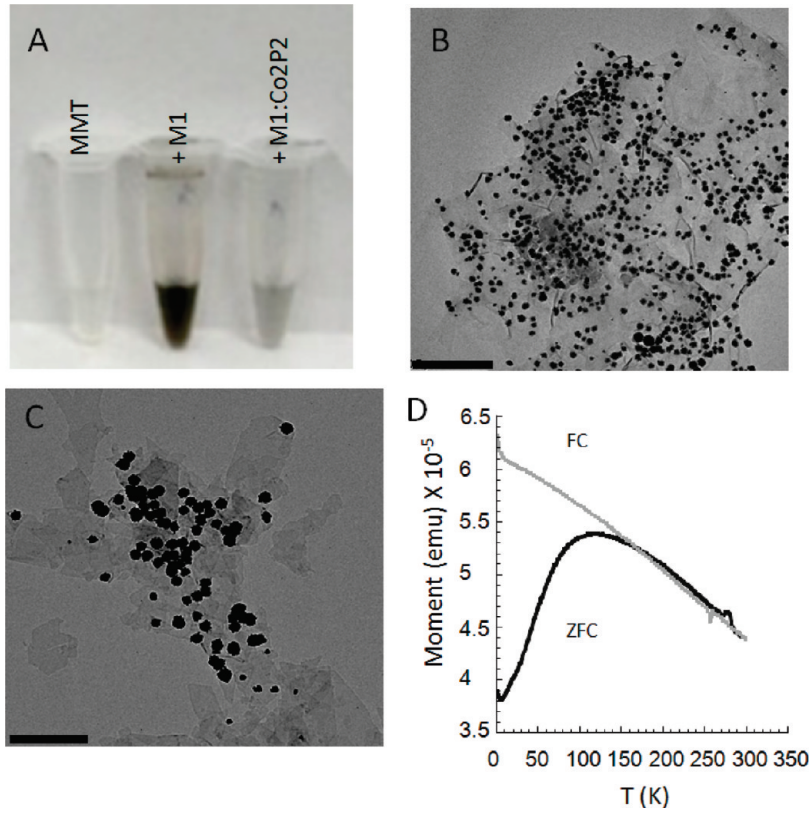

FIGURE 5. MMT-CoPt Nanohybrids. (A) Optical image of the CoPt-MMT hybrid suspensions: MMT only, CoPt-MMT produced using the M1 peptide, and CoPt-MMT produced using the M1-Co2P2 fusion peptide. TEM micrographs (200 kV) of CoPt-MMT hybrid nanoparticles produced using the (B) M1-Co2P2 fusion peptide or (C) M1 peptide. (D) Super quantum interference device (SQUID) magnetic property measurement from the CoPt-MMT hybrid nanoparticles produced using the M1 peptide. Scale bar 500 nm.

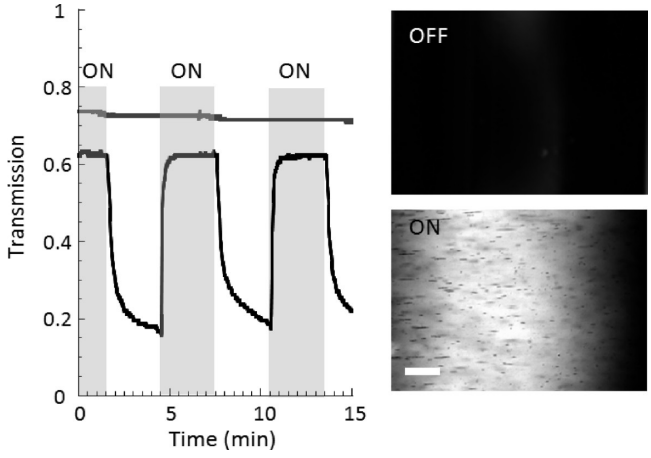

FIGURE 6. Optical switching of the CoPt-MMT hybrid nanoparticles using a magnet. Transmitted optical intensity through the CoPt-MMT (produced using the M1 peptide) as the field is applied and removed. The MMT suspension shows no significant transmission changes at a field strength of 0.2 T. Optical micrographs (right panels) through the CoPt-MMT (produced using the M1 peptide) as the field is applied (on) and removed (off). Scale bar 500 μm.

transmitted light intensity decreases (Figure 6). Optical micrographs obtained in the presence of a magnetic field showed translation of the MMT−CoPt nanohybrid, with an intermediate state of chain formation of the particles, finally resulting in the segregation of the nanohybrids to either ends of the light path resulting in ~60% of the transmitted light through the sample. Removal of the magnetic field results in the dispersion of the MMT-CoPt hybrids results in a decrease in optical transmission by ~66%, and this process was reversible over several cycles. MMT is a paramagnetic material and, depending on the source, contains a small amount of ferri- or antiferromagnetic iron impurities. Organically modified MMT in organic solvents has previously been shown to align in a magnetic field (48), however, only at much higher field strengths than used here. For MMT without magnetic modification, typically high field strengths of 1−9 T are necessary to observe any alignment effect.

In conclusion, we have identified peptides that bind to the surface of MMT sheets and the peptide interface can be used to create nanohybrids by localizing the growth of nanomaterials on the surface of the clay sheets. Using phage display, one peptide sequence was identified to bind to three types of modified MMT, and this sequence, M1, interacts through a cation exchange mechanism. The binding affinity found for the M1 peptide and the MMT surface (35 μM) would be advantageous for controlled release under certain environments, for example drugs or other molecules that released from the MMT surface in vivo. When fused to Au and CoPt binding peptides, M1 was still able to bind to the MMT surface, and the bifunctional peptides were able to direct metal nanoparticle growth at the MMT surface. These hybrid materials potentially offer a new route for fabricating clay hybrids that can be exploited in a number of applications such as biomedical, environmental, or multifunctional materials.

Acknowledgment. This work was funded by the Air Force Office of Scientific Research. The authors thank James O'Brien of Quantum Design for helpful discussions regarding magnetic property measurements and Melanie Tomczak, Marlene Houtz, and Justin Tomlin for technical assistance.

Supporting Information Available: Experimental procedures, phage display peptide isolation and analysis, and X-ray diffraction and thermogravimetric analysis (PDF). This material is available free of charge via the Internet at http://pubs.acs.org.

REFERENCES AND NOTES

(1) Brutchey, R. L.; Morse, D. E. *Chem. Rev.* **2008**, *108*, 4915–4934.
(2) Slocik, J. M.; Govorov, A. O.; Naik, R. R. *Angew. Chem., Int. Ed.* **2008**, *47*, 5335–5339.
(3) Park, S. Y.; Lytton-Jean, A. K. R.; Lee, B.; Weigand, S.; Schatz, G. C.; Mirkin, C. A. *Nature* **2008**, *451*, 553–556.
(4) Nykypanchuk, D.; Maye, M. M.; van der Lelie, D.; Gang, O. *Nature* **2008**, *451*, 549–552.
(5) Tomczak, M. M.; Gupta, M. K.; Drummy, L. F.; Rozenzhak, S. M.; Naik, R. R. *Acta Biomater.* **2009**, *5*, 876–882.
(6) Tamerler, C.; Sarikaya, M. *Philos. Trans. R. Soc. London, Ser. A* **2009**, *367*, 1705–1726.
(7) *Clay-Based Polymer Nanocomposites (CPN),CMS Workshop Lectures*; Carrado, K. A., Bergaya, F., Eds.; The Clay Minerals Society: Chantilly, VA, 2007; Vol. 15.
(8) Fusi, P.; Franci, M.; Ristori, G. G. *Appl. Clay Sci.* **1989**, *4*, 235–245.
(9) Liu, C.; Li, H.; Teppen, B. J.; Johnston, C. J.; Boyd, S. A. *Environ. Sci. Technol.* **2009**, *43*, 2777–2783.
(10) Churchman, G. J.; Gates, W. P.; Theng, B. K. G.; Yuan, G. In *Handbook of Clay Science*; Bergaya, F., Theng, B. K. G., Lagaly, G., Eds.; Elsevier: Amsterdam, 2006; pp 625—675.
(11) Causserand, C.; Kara, Y.; Aimar, P. *J. Membr. Sci.* **2001**, *186*, 165–181.
(12) Chih, T.; Hsi-Jung, J.; Wang, C. M. *J. Electroanal. Chem.* **2005**, *581*, 159–166.
(13) Baker, S. E.; Sawvel, A. P.; Zheng, N.; Stucky, G. D. *Chem. Mater.* **2007**, *19*, 4390–4392.
(14) Lozzi, I.; Calamai, L.; Fusi, P.; Bosetto, M.; Stotzky, G. *Soil Biol. Biochem.* **2001**, *33*, 1021–1028.
(15) Kalra, S.; Pant, C. K.; Pathak, H. D.; Mehata, M. S. *Colloid Surface A* **2003**, *212*, 43–50.
(16) Bujdák, J.; Rode, B. M. *J. Peptide Sci.* **2004**, *10*, 731–737.
(17) McLaren, A. D.; Peterson, G. H. *Soil Biochemistry*; Dekker: New York, 1967.
(18) Sanjay, G.; Sugunan, S. *J. Porous Mater.* **2007**, *14*, 127–136.
(19) Papp, S.; Patakfalvi, R.; Dékány, I. *Colloid Polym. Sci.* **2008**, *286*, 3–14.
(20) Drummy, L. F.; Koerner, H.; Phillips, D. M.; McAuliffe, J. C.; Kumar, M.; Farmer, B. L.; Vaia, R. A.; Naik, R. R. *Mater. Sci. Eng., C* **2009**, *29*, 1266–1272.
(21) Jacobs, J. D.; Koerner, H.; Heinz, H.; Farmer, B. L; Mirau, P.; Garrett, P. H.; Vaia, R. A. *J. Phys. Chem. B* **2006**, *110*, 20143–20157.
(22) Van Olphen, H. *An Introduction of Clay Colloid Chemistry*; John Wiley & Sons: New York, 1977.
(23) Theng, B. K. G. *The Chemistry of Clay—Organic Reactions*; Wiley: New York, 1974.
(24) Heinz, H.; Koerner, H.; Anderson, K. L.; Vaia, R. A.; Farmer, B. L. *Chem. Mater.* **2005**, *17*, 5658–5669.
(25) ExPASy proteomics server → Proteomics tools → Primary structure and analysis → MW, pI, Titration curve. (http://www.iut-arles.up.univ-mrs.fr/w3bb/d_abim/compo-p.html).
(26) Yariv, S.; Cross, H. *Organo—Clay Complexes and Interactions*; Marcel Dekker: New York, 2002.
(27) Cuadros, J.; Aldega, L.; Vetterlein, J.; Drickamer, K.; Dubbin, W. *J. Colloid Interface Sci.* **2009**, *333*, 78–84.
(28) Kwolek, Y.; Hodorowicz, M.; Stadnicka, K.; Czapkiewicz, J. *J. Colloid Interface Sci.* **2003**, *264*, 14–19.
(29) Kramer, R. A.; Cox, F.; van der Horst, M.; van der Oudenrijin, S.; Res, P. C.; Bia, J.; Logtenberg, T.; de Kruif, J. *Nucleic Acids Res.* **2003**, *31*, E59.
(30) Theng, B. K. G. *Formation and Properties of Clay—Polymer Complexes*; Elsevier: Amsterdam, 1979.
(31) Talibudeen, O. *Trans. Faraday Soc.* **1955**, *51*, 582–590.
(32) Wiess, A. In *Organic Geochemistry*; Eglinton, G., Murphy, M. T. J., Eds.; Springer: Berlin, 1969; pp 737—781.
(33) Pandey, R. B.; Heinz, H.; Feng, J.; Farmer, B. L.; Slocik, J. M.; Drummy, L. F.; Naik, R. R. *Phys. Chem. Chem. Phys.* **2009**, *11*, 1989–2001.
(34) Tamerler, C.; Sarikaya, M. *MRS Bull.* **2008**, *33*, 504–512.
(35) Hao, J.; Serohijos, A. W. R.; Newton, G.; Tassone, G.; Wang, Z.; Sgroi, D. C.; Dokholyan, N. V.; Basilion, J. P. *PLoS Comput. Biol.* **2008**, *4*, e1000138.
(36) Cannon, B.; Weaver, N.; Pu, Q.; Thiagarajan, V.; Liu, S.; Huang, J.; Vaughn, M. W.; Cheng, K. H. *Langmuir* **2005**, *21*, 9666–9674.
(37) Seker, U. O. S.; Wilson, B.; Sahin, D.; Tamerler, C.; Sarikaya, M. *Biomacromolecules* **2009**, *10*, 250–257.
(38) Hilnova, M.; Oren, E. E.; Seker, U. O. S.; Wilson, B. R.; Collino, S.; Evans, J. S.; Tamerler, C.; Sarikaya, M *Langmuir* **2008**, *24*, 12440–12445.
(39) Slocik, J. M.; Stone, M. O.; Naik, R. R. *Small* **2005**, *1*, 1048–1052.
(40) Diamanti, S.; Elsen, A.; Naik, R.; Vaia, R. *J. Phys. Chem. C* **2009**, *113*, 9993–9997.
(41) Szabo, T.; Bakandritsos, A.; Tzitzios, V.; Papp, S.; Korosi, L.; Galbacs, G.; Musabekov, K.; Bolatova, D.; Petridis, D.; Dekany, I. *Nanotechnology* **2007**, *18*, 285602.
(42) Bourlinos, A. B.; Delvin, E.; Boukos, N.; Simoppulos, A.; Petridis, D. *Clay Miner.* **2002**, *37*, 135–141.
(43) Mao, C.; Solis, D. J.; Reiss, B. D.; Kottman, S. T.; Sweeney, R. Y.; Hayhurst, A.; Georgiou, G.; Iverson, B.; Belcher, A. M. *Science* **2004**, *303*, 213–217.
(44) Naik, R. R.; Jones, S. E.; Murray, C. J.; McAullife, J. C.; Vaia, R. A.; Stone, M. O. *Adv. Funct. Mater.* **2004**, *14*, 25–30.
(45) Sanchez, J. M.; Morán-López, J. L.; Leroux, C.; Cadeville, M. C. *J. Phys. C: Solid State Phys.* **1988**, *21*, L1091–L1096.
(46) Kumbhar, A.; Spinu, L.; Agnoli, F.; Wang, K.-Y.; Zhou, W.; O'Connor, C. J. *IEEE Trans. Magn.* **2001**, *37*, 2216–2218.
(47) Chin, C.-J.; Yiacoumi, S.; Tsouris, C. *Colloids Surf.* **2002**, *204*, 63–72.
(48) Koerner, H.; Hampton, E.; Dean, D.; Turgot, Z.; Drummy, L.; Mirau, P.; Vaia, R. *Chem. Mater.* **2005**, *17*, 1990–1996.

AM1001184